IEEE Access
Multidisciplinary | Rapid Review | Open Access Journal

Received September 30, 2020, accepted October 9, 2020, date of publication October 15, 2020, date of current version October 28, 2020.

Digital Object Identifier 10.1109/ACCESS.2020.3031544

Primary Frequency Response of Microgrid Using Doubly Fed Induction Generator With Finite Control Set Model Predictive Control Plus Droop Control and Storage System

LUIS A. G. GOMEZ[1], (Member, IEEE), LUIS F. N. LOURENÇO[1], (Member, IEEE), AHDA P. GRILO[2], (Senior Member, IEEE), M. B. C. SALLES[1], (Member, IEEE), LASANTHA MEEGAHAPOLA[3], (Senior Member, IEEE), AND A. J. SGUAREZI FILHO[2], (Senior Member, IEEE)

[1]Laboratory of Advanced Electric Grids-LGrid, Polytechnic School, University of São Paulo (USP), São Paulo CO 05508-010, Brazil
[2]Center for Engineering, Modeling and Applied Social Sciences (CECS), Federal University of ABC (UFABC), Santo Andre CO 09210-580, Brazil
[3]RMIT University, Melbourne, VIC 3000, Australia

Corresponding author: Luis A. G. Gomez (alejandro.gutierrez@usp.br)

This work was supported in part by the University of São Paulo; in part by the Federal University of ABC; in part by the CAPES agency; in part by the CNPq agency (Process 405757/2018-2,305618/2017-2); and in part by the FAPESP agency (2017/04623-3, 2016/08645-9).

ABSTRACT This paper presents a new methodology for primary frequency response (PFR) in a microgrid through the finite control set-model predictive control (FCS-MPC) plus droop control applied to the grid side converter (GSC) of a doubly fed induction generator (DFIG). In this configuration, the rotor side converter (RSC) is responsible for maintaining wind turbine operation at the maximum power point (MPP) extraction, even at the time of a disturbance, while the GSC is responsible for processing the power required to reestablish the microgrid frequency at its rated value. The power required for frequency control comes from a battery energy storage system (BESS) connected to the DC-link, and its value is selected via the FSC-MPC by continuously adjusting the droop gain value. This control configuration has considerable benefits such as continuous operation at the MPP extraction, injection of power proportional to the frequency imbalance, the capability to impose restrictions through the control and it does not use any type of communication between the storage system and the control. Through the FCS-MPC, the gain of the droop controller is selected, which maximizes the power needed to control the frequency of the microgrid. To verify the performance of the proposed control strategy, simulations are performed for an unexpected islanding of the microgrid under different wind speed scenarios. The results show that the DFIG equipped with the proposed control strategy is able to provide ancillary services such as PFR in all DFIG operating modes.

INDEX TERMS Battery energy storage system (BESS), doubly fed induction generator (DFIG), droop control, finite control set-model predictive control (FCS-MPC), frequency control.

I. INTRODUCTION

Power generation from renewable energy sources, such as wind power, has increased year after year owing to technological advances and concerns on green-house gas emissions from conventional fossil fuel power generation [1]. Among wind power generation technologies, the doubly fed induction generator (DFIG) is one of the most widely used technology, given its variable-speed operation and independent control of active and reactive power [2]. Based on the common DFIG topology, the back-to-back converter is used for connecting the DFIG rotor to the grid, while the generator stator windings are connected directly to the grid. Due to the power electronic control of DFIG, they do not have an intrinsic response to grid frequency disturbances, and as a consequence, their output power does not change

The associate editor coordinating the review of this manuscript and approving it for publication was Xiaosong Hu.

according to changes in frequency although these disturbances are perceived by the converter controllers [3]. These frequency disturbances occur when there is an imbalance between the power generated by the generating units and the power consumed by the loads. In response to this imbalance, the synchronous generators connected to the system tend to maintain their speed and, as a result, their output power increases in order to reduce the power difference, and thus to return the frequency to its nominal value [4].

In this context, it is essential that wind generators and, in particular DFIG, have implemented control systems that allow them to participate in primary frequency response (PFR) by emulating the behavior of synchronous generators. There are already many research studies related to this aspect [5]–[16]. Research studies such as [5]–[8] use deloading to move the wind turbine from the maximum power point (MPP) extraction to ensure a stored power margin. Other studies such as [9]–[16] use the kinetic energy contained in the DFIG rotational masses, through inertia control or droop control, to inject an extra power. However, they all have three facts in common. The first is that the methods for getting DFIG to participate in frequency regulation are implemented in the rotor side converter (RSC), the second is that they all need to modify maximum power point tracking (MPPT) operation to be able to store power that will eventually be used to correct the frequency deviation, and the third aspect in common is that they use fixed switching frequency through pulse width modulation (PWM) to control power electronics. Since droop control could achieve better outcome [17], some studies, such as [18] present an approach considering variable droop control. This in order to obtain different support power values depending on the operating conditions.

Finite control set model predictive control (FCS-MPC) method applied to converters are presented in [19]–[25]. This method is supported by the fact that three-phase two-level converters have a finite number of switching states, and is characterized by predicting the behavior of the controlled variable by minimizing a cost function. From this statement, only a system model is required depending on the variables to be controlled. In [19]–[22], the general inverter topology, the system modeling, the definition of the cost function and the implementation of current control through the FCS-MPC are presented. Other researche studies such as [23]–[25] use the FCS-MPC applied to the DFIG RSC to control machine currents, power or torque. However, no previous articles addressed PFR of the DFIG using FCS-MPC, to the best of the knowledge of the authors.

In order to contribute to the studies carried out so far regarding the control of microgrids with high penetration of wind energy, this work proposes a coordinated control strategy for a DFIG equipped with BESS to provide PFR with variable droop characteristics through FCS-MPC. The proposed control strategy of this paper is innovative compared to the exiting strategies proposed in the literature due to following attributes:

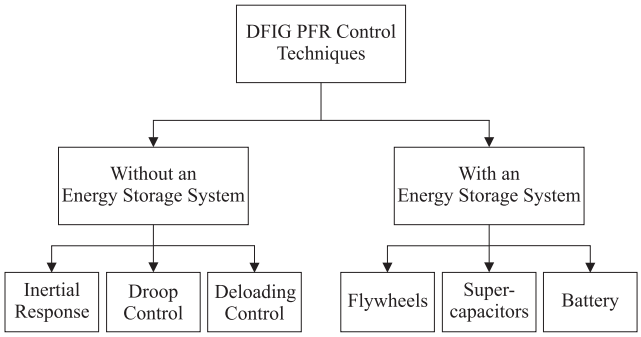

FIGURE 1. DFIG PFR control techniques.

1) Ensure the operation of the DFIG at the MPP extraction while it is providing PFR through the droop control implemented in the GSC and through the BESS connected to the DC-link.
2) Allow DFIG to provide PFR under low wind speeds. Due to the storage system connected to the DC-link, the DFIG can inject active power regardless of the wind speed at the moment of the disturbance.
3) Increase DFIG's ability to participate in PFR by dynamically adjusting the gain of the droop controller using the FCS-MPC. This feature will cause the DFIG to provide a more appropriate amount of active power, proportional to the power imbalance.
4) Grant the DFIG control system the freedom to place restrictions on its power output. Through the FCS-MPC it is possible to adjust the amount of active power available to provide PFR according to the requirements established by the power utilities.

II. THE PROBLEM DESCRIPTION

Variable-speed wind generators (VSWG), such as DFIG do not autonomously modify their active power output in response to variations in the grid frequency [26], [27]. This characteristic makes it impossible for DFIG to provide ancillary services as PFR in the event that the frequency of the electrical system requires it. Several alternatives have emerged around this area, based on the principle of centralized control that guarantees the balance of active power (generation and consumption). The research around DFIG is based on reproducing the behavior of synchronous generators, which is basically to inject an amount of extra power into the network after an unexpected frequency event, by adjusting the fuel in-feed according to the output power and monitoring the rotation speed itself.

As a result, the new challenges presented by DFIG to participate in PFR are: 1.) Enable DFIG to be able to perceive changes in the network, and 2.) Generate enough extra power to help restore the frequency of the system. To overcome these challenges, researchers have focused mainly on the methods presented in Figure 1 [28].

This section is structured as follows: subsection A presents the conventional DFIG control, and its inability to sense frequency variations in the grid; subsection B presents advances

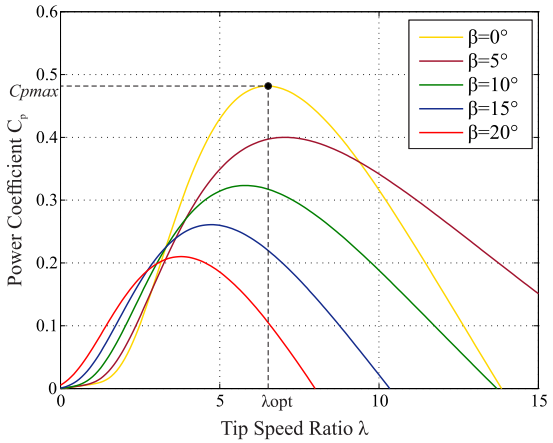

FIGURE 2. Tip speed ratio λ vs power coefficient C_P as a function of pitch angle β.

that allow DFIGs to participate in frequency control through control strategies; finally, subsection C outlines the proposed original contribution of this paper given the presented context.

A. CONVENTIONAL DFIG CONTROL

The expression that allows to calculate the power extracted by the wind turbine is presented in (1), where ρ is the air density (kg/m^3), A is the swept area by the blades (m^2), v_w is the wind speed (m/s) and C_p is the turbine power coefficient. C_p is specific to each turbine and its value depends on β, which corresponds to the pitch angle of the blades, and λ, known as the tip-speed ratio, described in (2). ω_r corresponds to the rotational speed of the turbine (rad/s) and R denotes the blade radius (m).

$$P_m = \frac{1}{2} \cdot \rho \cdot A \cdot v_w^3 \cdot C_p(\lambda, \beta) \tag{1}$$

$$\lambda = \frac{\omega_r \cdot R}{v_w} \tag{2}$$

Usually, the active power control is carried out by the DFIG rotor side converter (RSC) and is designed to operate at the MPP extraction through an maximum power point tracking (MPPT) strategy. For each wind speed v_w, there is a value of β and a value of ω_r at which the MPPT operation is achieved. If β is equal to zero ($\beta = 0°$), it will maximize the value of C_p. On the contrary, if the value of β is different from zero, the output power of the turbine will be lower when compared to $\beta = 0°$ for the same wind speed condition, as shown in Figure 2. For rotation ω_r to always be optimal for each wind speed, the torque τ must obey the τ_{opt} given by (3).

$$\tau_{opt} = K_{opt} \cdot \omega_r^2 \tag{3}$$

B. DFIG FREQUENCY REGULATION

According to research presented in [29], [30] there are several strategies that allow wind power generation systems equipped with DFIG to participate in the PFR. However, these strategies are fundamentally based on the idea of power reserve or "deloading", which guarantees DFIG to conserve part of its generation to later inject extra power in the presence of an event in the frequency. In line with the above, strategies can be classified into two categories. On the one hand are the methods that modify the pitch angle β, and on the other hand are the methods that use the kinetic energy stored in the rotating masses of the generator through over speed. In this work, the methods that use kinetic energy are analyzed. For more details about pitch angle deloading, the following references can be referred [31], [32].

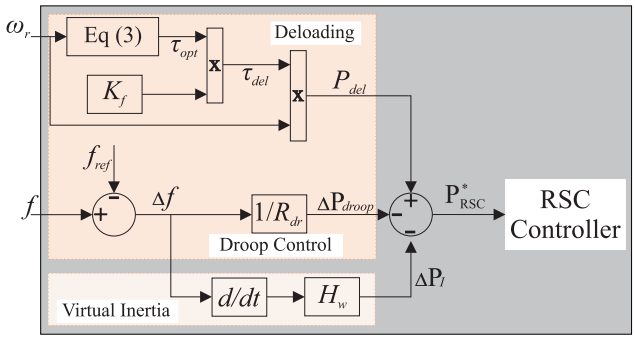

FIGURE 3. Conventional PFR control scheme.

1) ARTIFICIAL INERTIA RESPONSE, DELOADING AND DROOP CONTROL

The artificial inertia response method, also known as virtual inertia allows DFIG to reproduce the behavior of synchronous generators, providing active power support during frequency disturbances. This method uses the rate of change of frequency (ROCOF) to modify the reference torque provided by the MPPT. At the moment of the disturbance the torque increases causing the turbine to decelerate. However, this method is able to give support of power only in the phase of dynamic frequency variation. In view of this, another control loop must be added to the DFIG RSC in order to support active power for a longer period of time. This new control loop employs droop control to adjust the active power output depending on the frequency deviation, but needs to operate the turbine below the MPP extraction. Figure 3 shows the control block diagram.

According to Figure 3, the power that will be processed by the active power controller in the RSC is:

$$P^*_{RSC} = P_{MPPT} \cdot K_f - \Delta P_{droop} - \Delta P_I \tag{4}$$

where P_{MPPT} is the power generated by the MPPT strategy, K_f is the deloading factor ($P_{del} = P_{MPPT}.K_f$), ΔP_{droop} is the power generated by the droop control loop and is calculated from (5), and ΔP_I is the power generated by the virtual inertia loop. For the purpose of PFR, the virtual inercia response is ignored.

$$\Delta P_{droop} = \Delta f \cdot \frac{1}{R_{dr}} \tag{5}$$

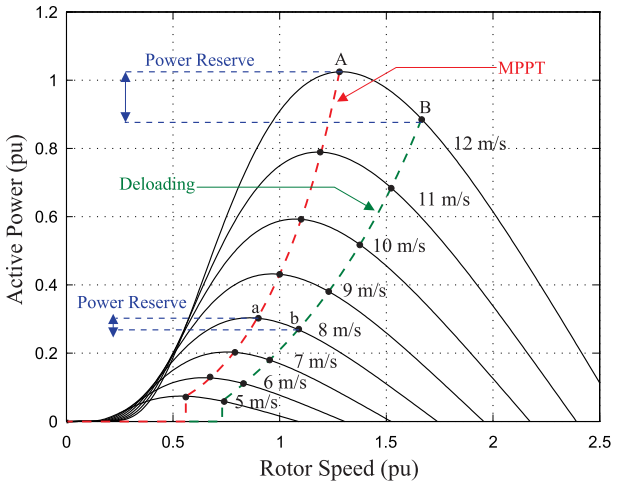

FIGURE 4. MPPT and deloading optimal power curves.

TABLE 1. Characteristics of DFIG operating modes.

	Operation Mode	
	MPPT	Deloading
Features	The turbine always delivers the maximum power available for each wind condition.	The turbine operates K_f times below optimal operation.
PFR Contribution	No	Yes
Stored Power	Kinetic energy	The amount of stored power depends on the K_f value and the wind speed.
Droop Control	It can be implemented using the kinetic energy contained in the rotating mass.	It can be implemented using the power reserve provided by deloading. It must be fulfilled that: $P_{MPPT}.K_f > \Delta P_{droop}$

In (4), the first term ($P_{MPPT}.K_f$) refers to the power that will be used for DFIG to participate in PFR. For this, the power generated through the MPPT is multiplied by the deloading factor K_f in order to generate the power reserve. This results in reduced power operation. Figure 4 shows the effect that the K_f factor has on MPPT.

The closer the K_f value is to 1, the smaller the displacement of the MPPT is, but also, the smaller the stored power margin will be. It is common to find $0.7 \leq K_f \leq 0.9$, or even in research studies such as in [33], perform simulations for $K_f = 0.6$ and $K_f = 0.5$, which means that a wind turbine will see its output power reduced, with the objective of providing frequency support. In other words, if a wind turbine generates $2MW$ operating with MPPT, its output power will be $1.94MW$ if $K_f = 0.8$ or $1.92MW$ if $K_f = 0.6$ (see Table 3), operating under deloading conditions, which makes this method inefficient.

If the wind speed is high, the DFIG operating under deloading conditions will, at best (the appropriate K_f value), have enough stored power to contribute to the PFR. But, what happens when the wind speed is low?. As shown in Figure 4, as the wind speed decreases (sub-synchronous operation), DFIG's ability to participate in PFR also decreases. When the wind speed is low, deloading does not acquire sufficient margin of stored power. In addition, the accuracy of the measurements will affect the stored power margin estimates (K_f value), since the DFIG operation under deloading depends on the measured wind speed.

The second term of (4) refers to the power obtained through the droop control loop. The droop controller consists of implementing an additional control loop within the DFIG active power control loop (RSC), in such a way that its response is proportional to the frequency deviation. In the case of DFIG, the droop control is used to generate a change in the active power injected by the generator when a frequency variation occurs. Therefore, the increment of active power injected by the droop control loop ΔP_{droop}, is proportional to the frequency variation of the system Δf and is inversely proportional to the droop gain R_{dr}, as presented in (5). Then, another factor of impact on the performance of DFIG is related to the correct choice of the gain of the droop control loop. Research studies [30], presents the calculation of $1/R_{dr}$ as:

$$\frac{1}{R_{dr}} = \frac{P_{rated}}{\delta \cdot f_r} \tag{6}$$

where P_{rated} is the nominal power of the generator, f_r is the nominal frequency of the system (50 or 60 Hz) and δ is the droop parameter. In [4], some of the values that can be used to calculate δ of the droop controller are presented. Depending on the requirements of the grid codes of each region, these values are selected. The stability of the DFIG while participating in the frequency regulation can be maintained through a high δ value. However, a high δ value means less ΔP_{droop}, that is, less participation in PFR. In [34], a δ value of 4% was used to calculate the gain of the droop control. In [35], the δ value is 7.14% and 2.77% in such a way that it fits under different operating conditions. The choice of these values is not justified in any research study. Another approach is presented in [36]. The authors in this work propose to implement a variable δ, in such a way that ΔP_{droop} adjusts to the oparation conditions. However, it needs the turbine to be in deloading operation.

The provision of ancillary services, such as PFR are increasingly essential in wind generators, such as DFIG. However, the methods used to give this characteristic to DFIG are not very efficient and their control parameters depend on variables, such as the wind. Table 1 summarizes the characteristics of the DFIG operating modes.

2) STORAGE SYSTEM

According to Figure 1, in addition to the methods that use deloading, another way to provide power support through DFIG is by using energy storage systems (ESS). The purpose of employing ESS is, on the one hand, to provide the active

power required to recover the speed of the generators and thus avoid a second frequency drop and, on the other hand, to serve as a support system in the event of a frequency drop [37]. In studies like [38], the authors use ESS based on flywheels connected to the point of common coupling (PCC) in order to provide frequency support. However, the operation of wind generators is under deloading in order to maintain a small power reserve. In general, storage systems based on flywheels use the kinetic energy contained in their rotating masses in order to provide some ancillary service, therefore, these systems must be large enough to support PFR. However, the costs of these systems can be high [39]. More information related to this type of systems are reported in [40], [41].

Another approach investigated by researchers is based on using the electrostatic energy contained in the capacitors to inject an extra power. Although capacitors initially in wind applications supported pitch control [42], there are currently applications in which supercapacitors are connected to the DC-link in order to provide ancillary services. It is a very interesting alternative since it does not require additional DC-DC converters, they are widely used to give inertia control but need to have some other system involved that can guarantee extra power to participate in PFR. With the use of supercapacitors, the GSC gains relevance in the system's power control. For more details about systems with supercapacitors, the reader is referred to [43]–[45].

On the other hand, there are systems that employ battery energy storage (BESS). Studies such as [46] presented a good panorama for BESS applied in renewable energy systems, and with the advancement of research on batteries (e.g. electric car), it is increasingly feasible to use this type of storage system in wind power applications to perform functions such as PFR [47], [48]. Around this subject, there are basically two types of BESS connections: on the one hand are the systems that use BESS connected to the PCC [37], [49]–[52] and on the other side are the systems that use BESS connected to the DC-link of the back-to-back converter [53]–[55]. Generally, systems with BESS connected to the PCC are used to support high power electrical systems, such as wind farms. However, connecting BESS to the PCC is not the best option, since the system would have a lot of transmission losses. In this case, the best option is to locate the BESS close to loads. Systems using BESS connected to the DC-link do not need inverters or communication systems between the turbine and the storage system, but the capacity of BESS is limited by the power that the converter can process.

3) GSC IN FREQUENCY REGULATION

From the point of view of standard operation, GSC is responsible for keeping the DC-link voltage constant in order to guarantee the power exchange between the generator and the network through the machine rotor, in such a way that the GSC will absorb power from the network (DC-link voltage drops) or inject power into it (DC-link voltage increases) depending on the DFIG operating mode, while the RSC takes action in response to the frequency imbalance. However as shown in the previous section, in some situations when storage systems connected to the back-to-back converter's DC-link are used, the GSC is responsible for controlling and managing the power generated, so that the generator provides ancillary services, while the turbine always operates at the MPP extraction. In most of these studies, the ESS is used to provide inertia control but in studies such as [56], the authors used BESS to provide PFR. The main feature here is that the active power used for frequency support is generated from a droop control loop. However, there is no clear methodology for calculating the gain of the droop control and regardless of the operating conditions, this value is fixed. Moreover, this method is not able to cope with power restrictions that might be established by the microgrid operator due to operating conditions.

C. PROBLEM STATEMENT AND CONTRIBUTION

As previously presented, conventional DFIG control aims at converting the maximum available power in the wind, following a MPPT strategy. This strategy makes it impossible for DFIG to react to frequency fluctuations. Hence, modifications to conventional control were proposed to overcome this limitation. The vast majority of the previously proposed control schemes relies on modifications to RSC's MPPT strategy. The frequency control strategy implemented on the GSC uses a fixed droop coefficient and is unable to cope with eventual constraints to the power flow.

Therefore, the original contribution of this work is the control strategy implemented in the GSC for managing the BESS, this allows the DFIG to participate in PFR of a microgrid, without operating outside the MPP, with an optimal droop coefficient and complying with power injection constraints that could be set by the microgrid operator. This strategy was implemented using finite control set-model predictive control (FCS-MPC) due to its superior capability to optimise gains as exemplified in the next section.

III. FINITE CONTROL SET-MODEL PREDICTIVE CONTROL IN FREQUENCY REGULATION

Finite control set-model predictive control (FCS-MPC) is a non-linear digital control strategy, which is simple to implement and suitable for energy conversion systems applications. Its control philosophy is based on predicting the future behavior of a control variable in each sample time by using the system model and select the optimal actuation based on the predefined optimization criteria [57]. The optimization parameters are related to the minimization of a cost function. FCS-MPC takes advantage of the finite number of switching states to predict possible states to minimize cost function [58]. In this way the FCS-MPC operates with a variable switching frequency that could be controlled by inserting restrictions in the cost function, if required by the operator.

It is increasingly common to find this digital control in wind energy conversion systems equipped with DFIG for ancillary service applications [59]. Due to the good performance of the FCS-MPC, DFIG can control the active power

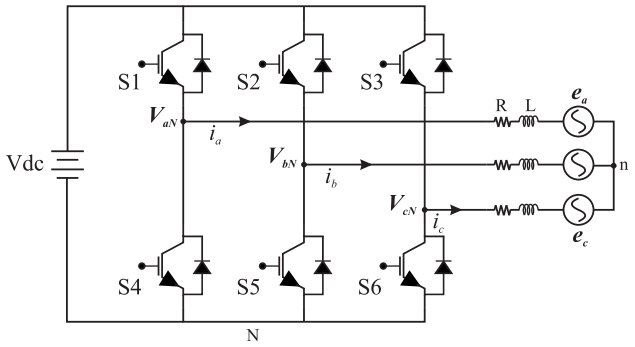

FIGURE 5. Inverter topology.

(among other variables) used to support frequency, optimizing a selection criterion through the converter's switching states. The steps associated with the FCS-MPC are summarized below.

A. INVERTER TOPOLOGY

The first step in implementing FCS-MPC is to model the inverter topology. Figure 5 presents the three-phase, two-level inverter. This inverter consists of a combination of six IGBTs-diode anti-parallel with only two possible states: completely ON or completely OFF. The number of possible switching states is determined from (7), where X is the number of possible states of each leg of the inverter, and y is the number of phases of the inverter.

$$N = X^y \tag{7}$$

Based on (7), the number of possible switching states for the three-phase, two-level inverter (Figure. 5) is 8 ($N = 2^3$), and the relationship between these switching states and the voltage vectors are presented in Table 2, where S_a, S_b and S_c are defined in (8), (9) and (10), respectively. Some possible switching states are not allowed:

- Both IGBTs in each phase are ON at the same time (short circuiting the DC-link).
- Both IGBTs in each phase are OFF at the same time (no power transfer).

$$S_a = \begin{cases} 1 \text{ if } S_1 \text{ ON and } S_4 \text{ OFF} \\ 0 \text{ if } S_1 \text{ OFF and } S_4 \text{ ON} \end{cases} \tag{8}$$

$$S_b = \begin{cases} 1 \text{ if } S_2 \text{ ON and } S_5 \text{ OFF} \\ 0 \text{ if } S_2 \text{ OFF and } S_5 \text{ ON} \end{cases} \tag{9}$$

$$S_c = \begin{cases} 1 \text{ if } S_3 \text{ ON and } S_6 \text{ OFF} \\ 0 \text{ if } S_3 \text{ OFF and } S_6 \text{ ON} \end{cases} \tag{10}$$

The inverter output voltage vector V can be described by (11) as a function of DC-link voltage and inverter switching states.

$$V = \frac{2}{3}(v_{aN} + a v_{bN} + a^2 v_{cN}) \tag{11}$$

TABLE 2. Switching states and voltage vectors.

State	S_a	S_b	S_c	Voltage Vector V
1	0	0	0	$V_0 = 0$
2	1	0	0	$V_1 = \frac{2}{3}V_{dc}$
3	1	1	0	$V_2 = \frac{1}{3}V_{dc}(1 + j\sqrt{3})$
4	0	1	0	$V_3 = \frac{1}{3}V_{dc}(-1 + j\sqrt{3})$
5	0	1	1	$V_4 = -\frac{2}{3}V_{dc}$
6	0	0	1	$V_5 = \frac{1}{3}V_{dc}(-1 - j\sqrt{3})$
7	1	0	1	$V_6 = \frac{1}{3}V_{dc}(1 - j\sqrt{3})$
8	1	1	1	$V_7 = 0$

where,

$$\begin{cases} v_{aN} = S_a V_{dc} \\ v_{bN} = S_b V_{dc} \\ v_{cN} = S_c V_{dc} \\ a = e^{j2\pi/3} \end{cases} \tag{12}$$

Transforming (11) into the stationary reference frame (α, β), we have:

$$\begin{aligned} V_\alpha &= \frac{2}{3}V_{dc}\left(S_a - \frac{1}{2}S_b - \frac{1}{2}S_c\right) \\ V_\beta &= \frac{2}{3}V_{dc}\left(\frac{\sqrt{3}}{2}S_b - \frac{\sqrt{3}}{2}S_c\right) \end{aligned} \tag{13}$$

Applying Kirchhoff's Voltage Law (KVL) to the inverter of Figure. 5, the equations representing the load current can be written as

$$\begin{aligned} v_{aN} &= i_a R + L\frac{di_a}{dt} + e_a \\ v_{bN} &= i_b R + L\frac{di_b}{dt} + e_b \\ v_{cN} &= i_c R + L\frac{di_c}{dt} + e_c \end{aligned} \tag{14}$$

where L is the load inductance and R is the load resistance. Substituting (14) into (11) and taking into account the load current given in (15) and the representation of the sources as motor back emf, the mathematical equation of the load is obtained and given by (16).

$$\begin{cases} i = \frac{2}{3}(i_a + a i_b + a^2 i_c) \\ e = \frac{2}{3}(e_a + a e_b + a^2 e_c) \end{cases} \tag{15}$$

$$v = Ri + L\frac{di}{dt} + e \tag{16}$$

B. DISCRETE-TIME MODEL

Once the equation representing the load current is defined to implement the FCS-MPC, it is required to discretize (16) for a

sampling time T_s. Thus, the discretized model will be used to predict the future value of the load current from the measured currents and voltages. By applying the Euler method on (16), the system model can be broadly represented by:

$$i(k+1) = \left(1 - \frac{T_s R}{L}\right) i(k) + \frac{T_s}{L}(v(k) - e(k)) \quad (17)$$

where $(k+1)$ represents the next sampling instant and (k) represents the current instant at which the last sampling state has been applied to the converter. $i(k)$ and $e(k)$ are the current and grid voltage measured, respectively, and can be written in the stationary reference frame (α, β) according to (18) and (19), respectively. Finally, $v(k)$ is the future value of the output voltage, determined by each voltage vector (switching states) applied to the converter. From (17), it is possible to predict the future value of the current at time $(k+1)$ for each one of the converter switch combinations.

$$\begin{aligned} i_\alpha(k) &= \frac{2}{3}\left(i_a - \frac{1}{2}i_b - \frac{1}{2}i_c\right) \\ i_\beta(k) &= \frac{2}{3}\left(\frac{\sqrt{3}}{2}i_b - \frac{\sqrt{3}}{2}i_c\right) \end{aligned} \quad (18)$$

$$\begin{aligned} e_\alpha(k) &= \frac{2}{3}\left(e_a - \frac{1}{2}e_b - \frac{1}{2}e_c\right) \\ e_\beta(k) &= \frac{2}{3}\left(\frac{\sqrt{3}}{2}e_b - \frac{\sqrt{3}}{2}e_c\right) \end{aligned} \quad (19)$$

Substituting (13), (18) and (19) to (17), the equation for current at the next sampling instant at the stationary reference frame (α, β) is:

$$i_{\alpha,\beta}(k+1) = \left(1 - \frac{T_s R}{L}\right) i_{\alpha,\beta}(k) + \frac{T_s}{L}(v_{\alpha,\beta}(k) - e_{\alpha,\beta}(k)) \quad (20)$$

From (20), the active and reactive powers that are injected into the grid at the next sampling time can be calculated as:

$$\begin{aligned} P_{(k+1)} &= \left[i_\alpha(k+1) \cdot e_\alpha + i_\beta(k+1) \cdot e_\beta\right] \\ Q_{(k+1)} &= \left[i_\alpha(k+1) \cdot e_\beta - i_\beta(k+1) \cdot e_\alpha\right] \end{aligned} \quad (21)$$

C. COST FUNCTION DEFINITION

In the FCS-MPC algorithm the current, voltage and powers injected into the grid, among other variables, can be controlled at the sample $(k+1)$. For this, once the converter has been modeled and the system has been discretized as a function of the variable to be controlled, a selection criterion must be defined. This criterion, known as the cost function (J), will evaluate each of the predicted values of the variables to be controlled for each switching state. The state that minimizes the cost function will be selected. Taking into account the (21), the cost function is defined as:

$$J = \left|P^*_{ref} - P_{(k+1)}\right| + \left|Q^*_{ref} - Q_{(k+1)}\right| \quad (22)$$

where, P_{ref} and Q_{ref} are the reference active and reactive power, respectively. The FCS-MPC strategy applied in the DFIG-GSC is based on the fact that the converter has only eight possible switching states. In addition, it is possible to model the system from the currents and the voltages measured in the grid in order to predict the behavior of the injected power through the switching states. Each of the eight switching states is evaluated in the power equation at sampling time $(k+1)$. Later these power values are processed by the cost function and the selected switching state will be the one that minimizes the function. Finally, this state is selected to drive the converter.

IV. THE PROPOSED SOLUTION

In this paper a new methodology for primary frequency regulation (PFR) of a microgrid using DFIG, BESS and FSC-MPC is presented. Motivated by the philosophy implemented in [60] where FCS-MPC is used to calculate the best position of the network angle, this article uses FCS-MPC to calculate the best gain of the droop control in accordance with the operating conditions. To accomplish the control targets, the BESS is responsible for providing the active power required to support frequency, while GSC is responsible for controlling the amount of active power.

A. FCS-MPC IN GSC

FCS-MPC was implemented in the GSC taking into account the structure shown in Figure 6. The control takes the grid currents and voltages in the $\alpha\beta$ frame and, through a system model, predicts the currents in the next sampling period. The predicted quantities for instant $k+1$ are used to calculate the predicted active and reactive powers. In addition, the controller takes the active power provided by the droop control as the reference active power. The development of FCS-MPC as a response to the frequency imbalance is shown in Figure 7 and is described below:

- In grid connected operation mode, the power exchange between the generator rotor and the grid will depend on the DFIG operation mode. If the wind speed is below the synchronous speed (sub-synchronous operation), the rotor needs to absorb power to keep the DC-link voltage constant, but if the wind speed is above the synchronous speed (super-synchronous operation), DFIG GSC supplies power generated through the rotor. In both cases, the reference power calculated from the droop control is zero, so the FCS-MPC selects the states that satisfy this operating condition.
- As soon as the disturbance occurs and the system starts to operate in microgrid mode, Δf is different from zero and the predictive control takes action. The control starts by evaluating the voltage of the DC-link and the grid voltage and current values. It initializes the variables that contain the values of the switching states i, the parameters of the droop control (reference power P^*_{ref}) and the restrictions if applicable.
- Applying (6), a value for δ is selected in such a way that together with Δf they are able to calculate the P_{opt}

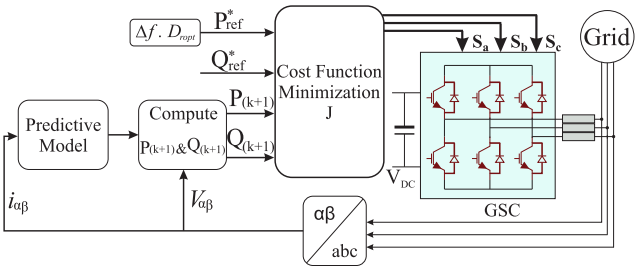

FIGURE 6. Block diagram of the proposed GSC FCS-MPC.

power. The higher the value of the P^*_{ref}, the greater the participation of DFIG in PFR. For this reason, the controller compares the value of the previously calculated P_{opt} power with the value stored in P^*_{ref} and updates the value of P^*_{ref} each time the condition $P_{opt} > P^*_{ref}$ is fulfilled. It must be taken into account that if there are restrictions, the P^*_{ref} value will be updated if the condition of the restrictions $P_{lim} > P^*_{opt}$ is also met.

- Once P^*_{ref} value is updated and saved, the controller evaluates the system model (equation 20) for all possible switching states to predict the future value of the current at the instant $(k+1)$. For this step, the first value of the voltage vector $V(k)$ in Table 2 is selected. This value is used together with the current and voltage grid values (instant k) to predict the current at the instant $(k+1)$ and also the active and reactive powers $P(k+1)$ and $Q(k+1)$, respectively.
- Once the active and reactive powers are calculated (in this case we are only analyzing $P(k+1)$), the control evaluates the cost function J, that is compared with the stored minimal value J_0. If $J < J_0$, then the minimal value J_0 is updated; in other words, the cost function J will be minimized. When all the values of $V(k)$ have been evaluated and the lowest value of J has been stored, the program evaluates the following δ value and calculates a new P_{opt} value to later make the same sequence presented above. Finally, once all the δ and $V(k)$ values have been analyzed and evaluated throughout the control, the FCS-MPC algorithm provides as output the switching state and the δ value minimized the cost function.

B. BESS CONNECTED TO THE DC-LINK

In this paper BESS was directly connected to the DC-link of the back-to-back converter through a buck-boost converter as shown in Figure 8. With this configuration the objective is to control the voltage of the DC-link through the battery converter so that the power required for frequency regulation was injected directly into the converter, without using any communication system. For wind speeds above the synchronous generator speed ($11m/s$), the DC-link voltage will start to increase, in which case the battery absorbs the extra power. On the other hand, if the wind speed is below the rated speed, BESS injects the necessary power to keep the DC-link voltage constant.

V. DESCRIPTION OF THE STUDIED SYSTEM

In order to study the impact of the FCS-MPC method implemented in the DFIG GSC for frequency regulation in a microgrid, the typical medium voltage distribution system presented in Figure 9 was adopted. Initially, the microgrid composed of the DFIG-BESS, the synchronous generator (SG) and the loads of constant value over time connected in the $B1-B5$ buses are connected to the grid. After a period of time, this system is isolated from the network. The total active and reactive power consumed by the loads of the microgrid are $P_{tot} = 3.20135MW$ and $Q_{tot} = 695kW$, respectively. The power consumed by the loads is considered constant, since these values represent the value of heavy load in this system. These values correspond to the time of the day of maximum power consumption on each busbar. The synchronous generator has a rated power of $P_{S.G} = 3.3MVA$ and the nominal power of the DFIG is $P_{DFIG} = 2MVA$. Connected to the DC-link of the back-to-back converter, there is a lithium-ion battery with nominal power of 700 kW, rated current of $4000A$ and rated voltage of $250V$. The DC-link voltage and frequency of the system are $1150V$ and $60Hz$, respectively.

VI. SIMULATION RESULTS

Initially, the DFIG-BESS and SG are operating connected to the main grid, as shown in Figure 9. After a while (30 s), the breaker opens and the DFIG-BESS and SG are running on a microgrid, feeding the loads $C1 - C6$. The moment the breaker opens, a power imbalance occurs which causes the frequency to decrease. In order to share efforts with SG in frequency regulation, DFIG via droop control and FSC-MPC, in a controlled way, increases its active power output. To analyse the proposed strategy under various operating conditions, wind speeds were chosen to represent 30% of the synchronous speed (up and down). In this way, the DFIG operation cover super synchronous, synchronous and sub-synchronous operating modes. Thus, the wind speeds (V_s) used in the simulations are $8m/s$, $11m/s$ and $14m/s$.

As it was presented throughout this work, one of the main advantages of the proposed configuration is to guarantee the operation of the DFIG at the MPP extraction at all times, including during frequency disturbances. In Figure 10 the comparison is made between the output power of the DFIG operating with MPPT and with a delaoding factor of $K_f = 0.6$, for a wind speed of $v_w = 13m/s$

According to Figure 10, under MPPT operation the power that DFIG supplies to the grid is greater than 0.8 pu, whereas if DFIG is operating with deloading its output power is below 0.7 pu. In general terms, for DFIG to participate in PFR using the traditional method (deloading), its output power has to be reduced in order to have a stored power margin. Table 3 shows the nominal power output for each wind speed, the output power applying two k_f values and the respective stored power margin.

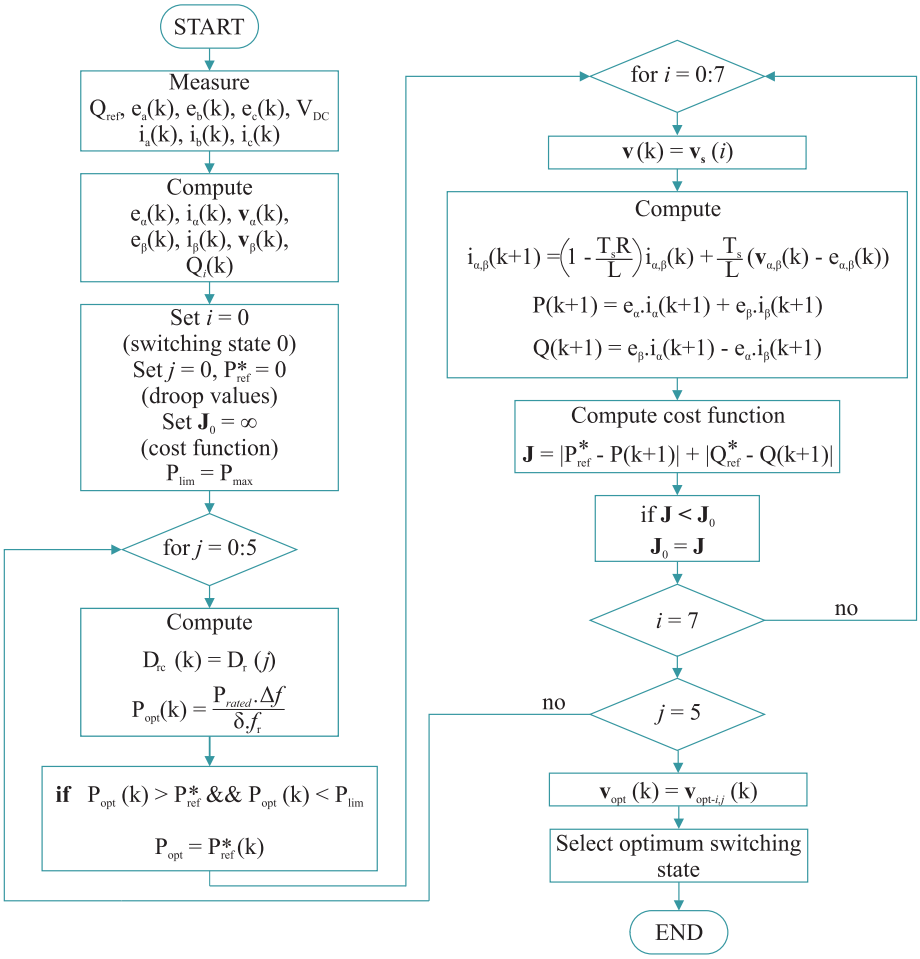

FIGURE 7. Flowchart of the proposed FCS-MPS algorithm.

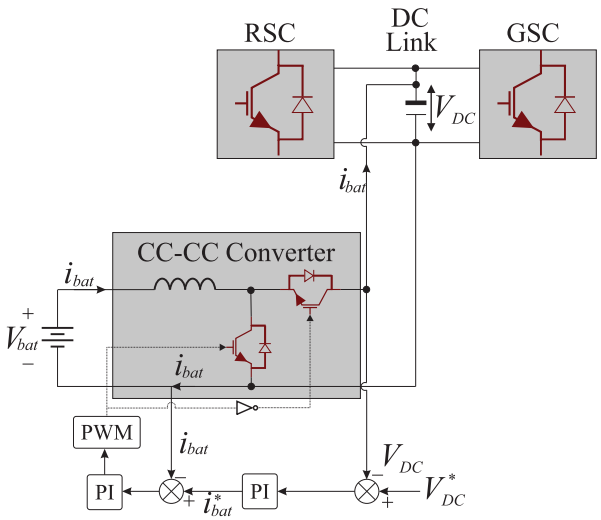

FIGURE 8. BESS control block diagram.

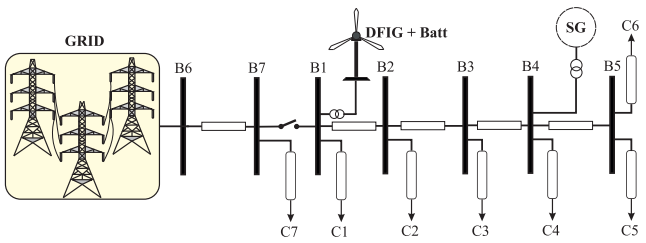

FIGURE 9. General distribution system.

A. FCS-MPC PLUS DROOP CONTROL AND BESS RESULTS

The microgrid operation is quite laborious given its low reaction capacity in the face of external disturbances and can become even more challenging in the presence of low wind speeds. In this case, a disturbance in the frequency can easily destabilize the microgrid completely, since the difference between the generated and consumed power is large. In order for this not to happen, synchronous units must increase their participation. As a result of this action, the frequency may fluctuate a few seconds and take a few more seconds before returning to its nominal value. This behavior can be seen in the yellow graph in Figure 11. Figure 11 shows the behavior of the microgrid frequency, after sudden opening of the breaker at $t = 30s$, for a wind speed of $v_w = 8m/s$.

However, by implementing FCS-MPC plus droop control in the GSC of DFIG and connecting BESS to the DC-link,

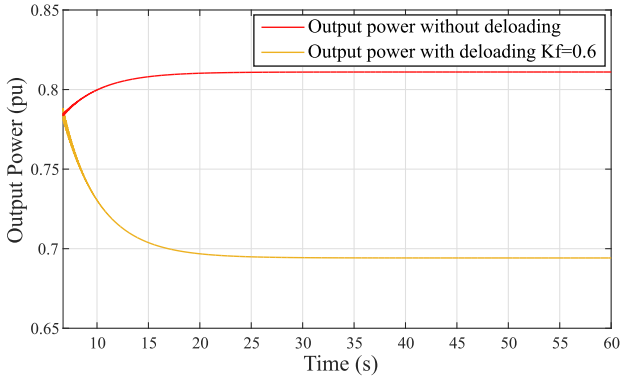

FIGURE 10. DFIG output power for $v_w = 13m/s$.

TABLE 3. Switching states and voltage vectors.

Wind Speed [m/s]	DFIG Rated Power Output [pu]	DFIG Power Output with $K_f = 0.8$ [pu]	Power Reserve with $K_f = 0.8$ [pu]	DFIG Power Output with $K_f = 0.6$ [pu]	Power Reserve with $K_f = 0.6$ [pu]
14	1	0.97	0.03	0.962	0.038
13	0.811	0.777	0.034	0.6942	0.1168
12	0.637	0.611	0.026	0.5466	0.0904
11	0.49	0.471	0.019	0.4213	0.0687
10	0.368	0.351	0.017	0.3165	0.0515
9	0.2676	0.2574	0.0102	0.2305	0.0371
8	0.1874	0.1803	0.0071	0.16	0.0274

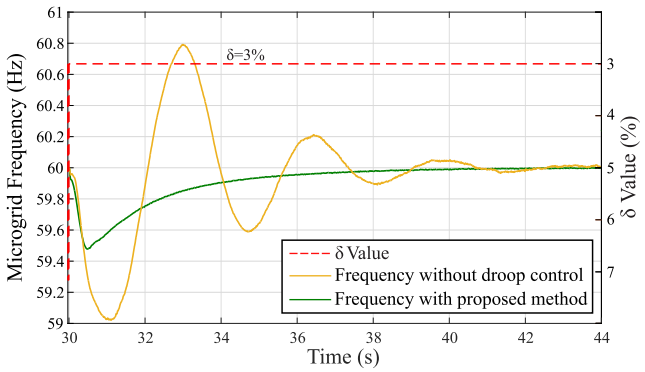

FIGURE 11. Microgrid frequency response for $v_w = 8m/s$.

the frequency of the microgrid did not show any oscillations, lower nadir value and returned to its nominal value 5s faster. This performance was achieved because ΔP_{droop} value was maximized through the FCS-MPC. Through the control, all δ values were analyzed and the value that minimized the cost function was selected, in this case, the value was $\delta = 3\%$ as shown in the red dotted graph. This δ value was used by the control until the frequency returned to its nominal value.

Figure 12 shows BESS performance, the power processed by the GSC and the power supplied by the DFIG to the

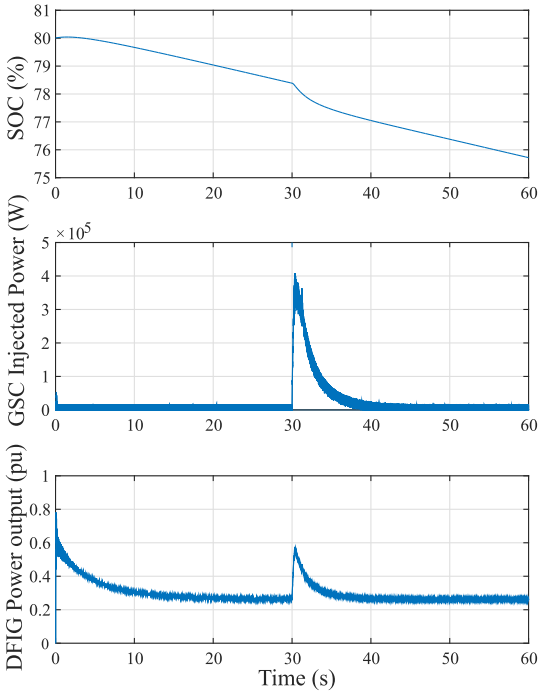

FIGURE 12. SOC, GSC power and DFIG output power for $v_w = 8m/s$.

microgrid at all times. Since the DFIG is operating at sub-synchronous mode, the BESS provides power in order to keep the DC-link voltage constant, but when the disturbance occurs, the BESS provides 400kW, via the FCS-MPC plus droop control to control the frequency. By comparing this power value with the stored power for $K_f = 0.6$ deloading value for the same wind speed, (54.8kW taking the base value 2MW, Table 3), the available power reserve with deloading is insufficient for DFIG to participate in the PFR.

As the wind speed increases, the power generated by the DFIG and subsequently injected into the grid also increases. This causes the difference between the generated power and the consumed power to decrease and consequently the frequency imbalance also decreases. In the situation shown in Figure 13, the wind speed is 11m/s and once again the proposed method was able to improve the frequency response in the presence of a disturbance, maintaining the same control philosophy as in the previous case. To maximize the ΔP_{droop} value, the controller selected $\delta = 3\%$.

The result of the control over the frequency of the microgrid is positive since the frequency does not present oscillations and the frequency nadir improves by approximately 0.4 Hz. However, the power value provided by BESS was much lower when compared with the previous case. As shown in Figure 14, the battery discharge is minimal, showing a power output of 125kW. Before the disturbance and under normal operating conditions, the power output of the DFIG was 0.5pu and the SOC of the battery practically constant. When the disturbance occurs, the battery injects the power required by the FCS-MPC and which is necessary to control the frequency. As the frequency returns to its nominal value, the power processed by the GSC returns to zero and the power

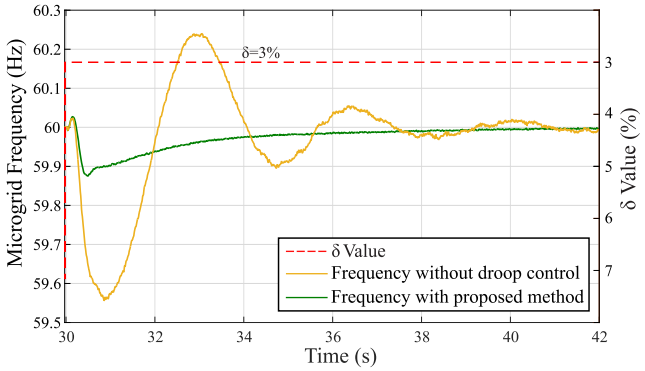

FIGURE 13. Microgrid frequency response for $v_w = 11m/s$.

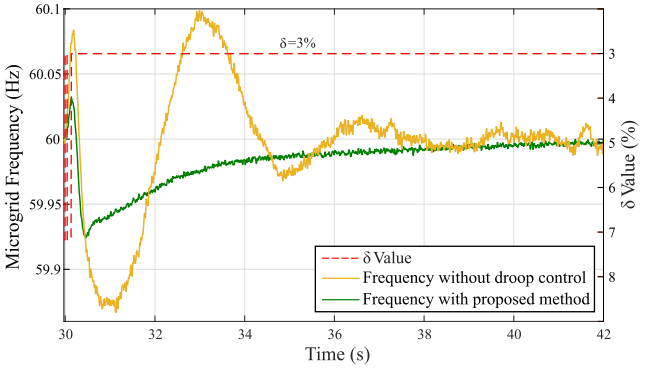

FIGURE 15. Microgrid frequency response for $v_w = 14m/s$.

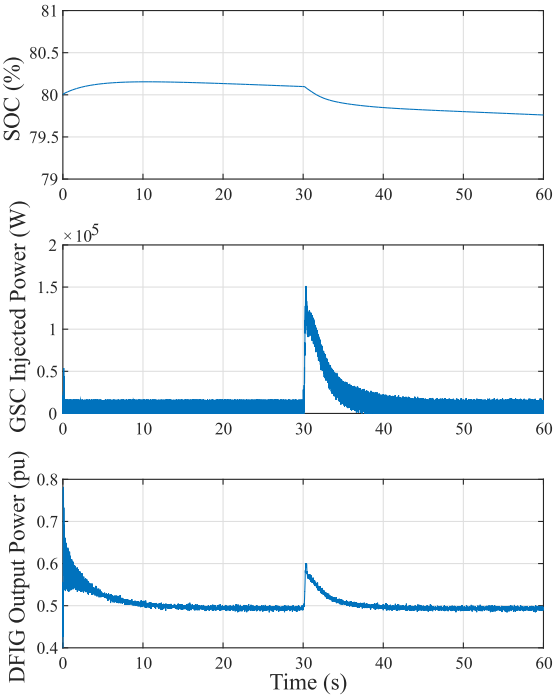

FIGURE 14. SOC, GSC power and DFIG output power for $v_w = 11m/s$.

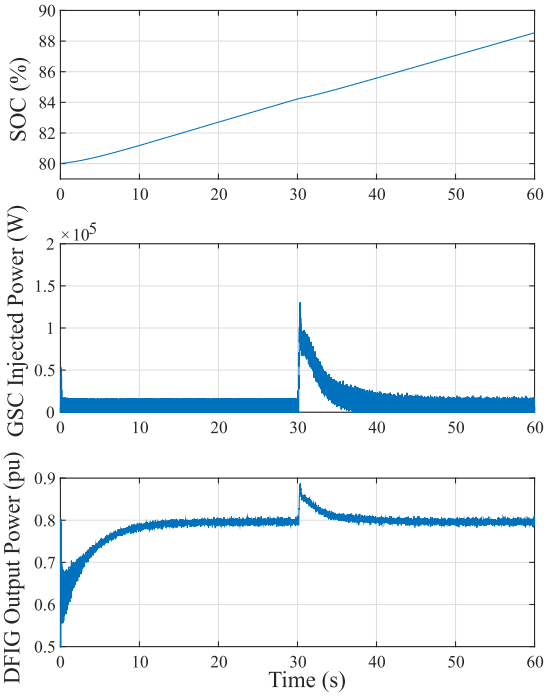

FIGURE 16. SOC, GSC power and DFIG output power for $v_w = 14m/s$.

injected by the DFIG remains at $0.5pu$. Even using the stored power with $K_f = 0.6$ (deloading control), the contribution of PFR by the DFIG is at the limit.

For super-synchronous operation the control conditions are less demanding. With the DFIG operating at its rated speed ($v_w = 14m/s$), the power generation is injected through the stator, but also through the machine's rotor. This makes the difference between the generated and consumed power even smaller compared to the two cases previously analyzed. As shown in Figure 15, in these operating conditions, the frequency nadir has been improved by approximately $0.1\ Hz$ and without oscillations. The same value of $\delta = 3\%$ was selected to minimize the cost function.

Since part of the generated power flows through the machine's rotor, the DC-link voltage tends to increase. For this reason the power that passes through the DC-link is used to charge the battery, as shown in Figure 16. This same analysis can be used to explain the behavior of the DFIG's power output. In the event that the state of charge of the BESS was fully charged ($SOC = 100\%$), the power generated by the DFIG that flows through the rotor is entirety injected into the grid and the power output would be $1pu$. When the disturbance occurs, the FCS-MPC asked the battery for approximately $110kW$ to control the frequency and after that the BESS continues to charge.

With the FCS-MPC plus droop control method, implemented in the GSC and BESS connected to the DC-link, it was possible to control the frequency of the microgrid even under low wind conditions. The controller calculates the power proportional to the frequency deviation and chooses the appropriate combination of switching states, once the cost function has been minimized. In the cases previously analyzed, the δ value to calculate the gain of the droop control was always 3% given that the main requirement was to maximize the ΔP_{droop} value. One of the advantages of using the proposed method is that it allows DFIG to participate in the

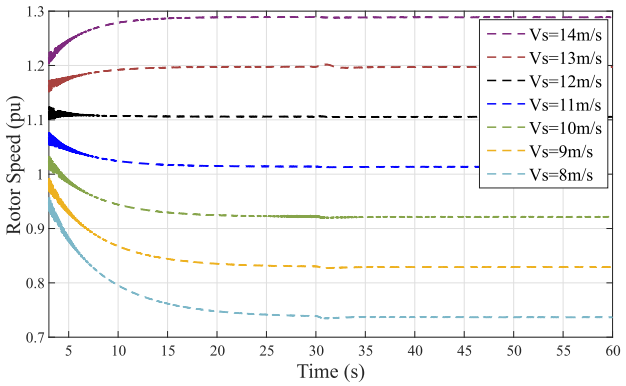

FIGURE 17. DFIG rotor speed.

PFR without affecting operation at the MPP. Figure 17 shows that the DFIG is always at the nominal rotation according to each wind speed, even when the disturbance occurs.

B. FCS-MPC PLUS DROOP CONTROL WITH CONSTRAINTS

Another main advantage of the FCS-MPC over other types of control (e.g. linear control) is that it allows you to insert constraints to be taken into account when the cost function is minimized in case the grid operator indicates a maximum or minimum power limit, or even to safeguard the equipment. Particularly in this work, the constraint can be inserted in such a way that it regulates the value of the power supplied for the frequency control, ΔP_{droop} according to a system parameter. In response, the controller will select the δ value that meets the constraint.

When the disturbance occurs, the proposed control is responsible for selecting the δ value, that makes the ΔP_{droop} value to the maximum, in such a way that the participation of DFIG in PFR is greater. However, some constraints can be added as shown in Figure 18. Here, the constraint consisted of maximizing the ΔP_{droop} value without exceeding an established value for the GSC ($300kW$). In this way, the controller evaluates all possible δ values and chooses the value that generates the maximum ΔP_{droop} value, and that does not exceed $300kW$. Since the analyzed wind speed is very low, care must be taken not to too much limit the power of the converter. In order to satisfy this requirement, the δ value selected to operate in the most critical part of the disturbance was 4%. In Figure 18, it can be seen that the control can satisfy the constraint without neglecting the frequency control.

In the case where the wind speed is 11 m/s, the behavior of the δ value was different compared to the δ for the wind speed of 8 m/s, as shown in Figure 19, since the constraint has changed. In this case, the power limit defined by the GSC was $110kW$. In order to not to exceed this power value, the first δ value was set at 6% and as the frequency returned to its nominal value, δ values were set at 5%, 4% and 3%, respectively. In the same way as in the previous case, the control allows controlling the frequency taking into account the power constraint.

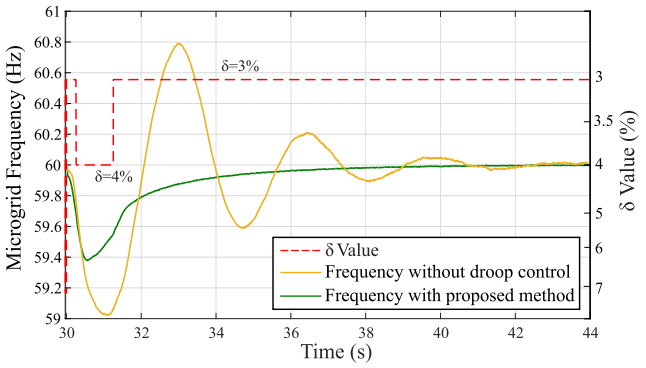

FIGURE 18. Microgrid frequency response for $v_w = 8m/s$ with constraints.

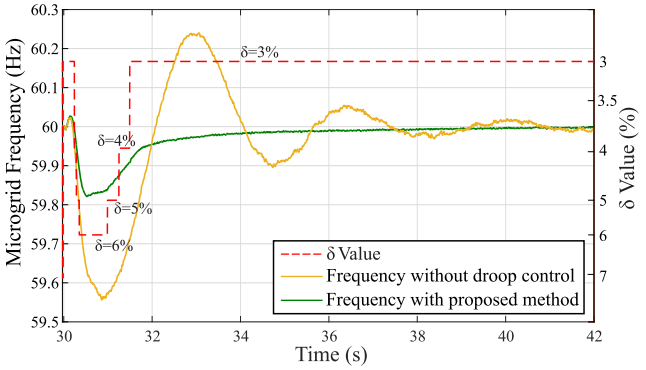

FIGURE 19. Microgrid frequency response for $v_w = 11m/s$ with constraints.

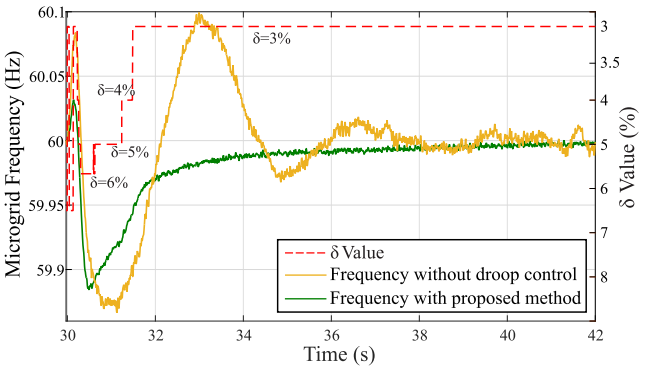

FIGURE 20. Microgrid frequency response for $v_w = 14m/s$ with constraints.

Finally for super-synchronous operation, the power of the GSC was restricted to $80kW$. As shown in Figure 20, the δ values that met the constraint by keeping the frequency of the microgrid controlled within acceptable value were 6%, 5%, 4% and 3%. As the frequency returns to its nominal value, the ΔP_{droop} value is maximized.

VII. CONCLUSION

A new methodology for primary frequency response of a microgrid through FSC-MPC plus droop control implemented in DFIG GSC and BESS connected to the DC-link has been proposed in this study. This method ensures the operation at the point of maximum power extraction while the DFIG provides PFR. The use of a storage system enabled

DFIG to provide active power even in sub-synchronous operation, since it does not have the power limits even under deloaded operation. Likewise, the proposed FCS-MPC plus droop control ensured DFIG to provide the exact amount of active power, depending on operating conditions or system constraints. Modifying the gain value of the droop control and/or placing restrictions directly on the control, allows wind generation systems to adjust more quickly to changes experiencing by the electrical systems. The proposed controller exhibits improved PFR, under any wind condition, hence provides better frequency regulation. Proposed scheme also provides PFR up to 5s for sub-synchronous operation and completely eliminates oscillations in all DFIG operation modes.

REFERENCES

[1] *Renewable Energy Policies in a Time of Transition*, IEA IRENA, Paris, France, 2018, pp. 62–64, vol. 4. Accessed: Nov. 17, 2019. [Online]. Available: https://www.irena.org/-/media/Files/IRENA/Agency/Publication/2018/Apr/IRENA_IEA_REN21_Policies_2018.pdf

[2] B. Jain, S. Jain, and R. K. Nema, "Control strategies of grid interfaced wind energy conversion system: An overview," *Renew. Sustain. Energy Rev.*, vol. 47, pp. 983–996, Jul. 2015.

[3] D. Yang, J. Kim, Y. C. Kang, E. Muljadi, N. Zhang, J. Hong, S.-H. Song, and T. Zheng, "Temporary frequency support of a DFIG for high wind power penetration," *IEEE Trans. Power Syst.*, vol. 33, no. 3, pp. 3428–3437, May 2018.

[4] C. Roberts, "Review of international grid codes," Tech. Rep., 2018.

[5] V. Gholamrezaie, M. G. Dozein, H. Monsef, and B. Wu, "An optimal frequency control method through a dynamic load frequency control (LFC) model incorporating wind farm," *IEEE Syst. J.*, vol. 12, no. 1, pp. 392–401, Mar. 2018.

[6] J. Zhao, X. Lyu, Y. Fu, X. Hu, and F. Li, "Coordinated microgrid frequency regulation based on DFIG variable coefficient using virtual inertia and primary frequency control," *IEEE Trans. Energy Convers.*, vol. 31, no. 3, pp. 833–845, Sep. 2016.

[7] U. Datta, J. Shi, and A. Kalam, "Primary frequency control of a microgrid with integrated dynamic sectional droop and fuzzy based pitch angle control," *Int. J. Elect. Power Energy Syst.*, vol. 111, pp. 248–259, Oct. 2019.

[8] Y. Tan, L. Meegahapola, and K. M. Muttaqi, "A suboptimal power-point-tracking-based primary frequency response strategy for DFIGs in hybrid remote area power supply systems," *IEEE Trans. Energy Convers.*, vol. 31, no. 1, pp. 93–105, Mar. 2016.

[9] Y. Han and J.-I. Ha, "Droop control using impedance of grid-integrated DFIG within microgrid," *IEEE Trans. Energy Convers.*, vol. 34, no. 1, pp. 88–97, Mar. 2019.

[10] J. Van De Vyver, J. D. M. De Kooning, B. Meersman, L. Vandevelde, and T. L. Vandoorn, "Droop control as an alternative inertial response strategy for the synthetic inertia on wind turbines," *IEEE Trans. Power Syst.*, vol. 31, no. 2, pp. 1129–1138, Mar. 2016.

[11] E. Muljadi, V. Gevorgian, M. Singh, and S. Santoso, "Understanding inertial and frequency response of wind power plants," in *Proc. IEEE Power Electron. Mach. Wind Appl.*, Jul. 2012, pp. 1–8.

[12] A. S. Ahmadyar and G. Verbic, "Coordinated operation strategy of wind farms for frequency control by exploring wake interaction," *IEEE Trans. Sustain. Energy*, vol. 8, no. 1, pp. 230–238, Jan. 2017.

[13] Y. Li, Z. Xu, J. Ostergaard, and D. J. Hill, "Coordinated control strategies for offshore wind farm integration via VSC-HVDC for system frequency support," *IEEE Trans. Energy Convers.*, vol. 32, no. 3, pp. 843–856, Sep. 2017.

[14] A. S. Ahmadyar and G. Verbic, "Control strategy for optimal participation of wind farms in primary frequency control," in *Proc. IEEE Eindhoven PowerTech*, Jun. 2015, pp. 1–6.

[15] M. F. M. Arani and Y. A.-R.-I. Mohamed, "Analysis and impacts of implementing droop control in DFIG-based wind turbines on microgrid/weak-grid stability," *IEEE Trans. Power Syst.*, vol. 30, no. 1, pp. 385–396, Jan. 2015.

[16] Y.-L. Hu and Y.-K. Wu, "Approximation to frequency control capability of a DFIG-based wind farm using a simple linear gain droop control," *IEEE Trans. Ind. Appl.*, vol. 55, no. 3, pp. 2300–2309, May 2019.

[17] L. A. G. Gomez, B. G. Bueno, A. P. Grilo, A. J. S. Filho, and M. Salles, "Analysis of the doubly fed induction generator performance on frequency support of microgrids," in *Proc. North Amer. Power Symp. (NAPS)*, Sep. 2017, pp. 1–6.

[18] M. Garmroodi, G. Verbic, and D. J. Hill, "Frequency support from wind turbine generators with a time-variable droop characteristic," *IEEE Trans. Sustain. Energy*, vol. 9, no. 2, pp. 676–684, Apr. 2018.

[19] R. N. Fard, "Finite control set model predictive control in power converters," M.S. thesis, Institutt elkraftteknikk, Trondheim, Norway, 2013.

[20] S. Vazquez, J. Rodriguez, M. Rivera, L. G. Franquelo, and M. Norambuena, "Model predictive control for power converters and drives: Advances and trends," *IEEE Trans. Ind. Electron.*, vol. 64, no. 2, pp. 935–947, Feb. 2017.

[21] J. Rodriguez, M. P. Kazmierkowski, J. R. Espinoza, P. Zanchetta, H. Abu-Rub, H. A. Young, and C. A. Rojas, "State of the art of finite control set model predictive control in power electronics," *IEEE Trans. Ind. Informat.*, vol. 9, no. 2, pp. 1003–1016, May 2013.

[22] H. A. Young, M. A. Perez, and J. Rodriguez, "Analysis of finite-control-set model predictive current control with model parameter mismatch in a three-phase inverter," *IEEE Trans. Ind. Electron.*, vol. 63, no. 5, pp. 3100–3107, May 2016.

[23] P. Kou, D. Liang, J. Li, L. Gao, and Q. Ze, "Finite-control-set model predictive control for DFIG wind turbines," *IEEE Trans. Autom. Sci. Eng.*, vol. 15, no. 3, pp. 1004–1013, Jul. 2018.

[24] A. J. S. Filho and E. R. Filho, "Model-based predictive control applied to the doubly-fed induction generator direct power control," *IEEE Trans. Sustain. Energy*, vol. 3, no. 3, pp. 398–406, Jul. 2012.

[25] R. V. Jacomini and A. J. S. Filho, "Finite control set applied to the direct power control of a DFIG operating under voltage sags," *IEEE Trans. Sustain. Energy*, vol. 10, no. 2, pp. 952–960, Apr. 2019.

[26] D. Ochoa and S. Martinez, "Fast-frequency response provided by DFIG-wind turbines and its impact on the grid," *IEEE Trans. Power Syst.*, vol. 32, no. 5, pp. 4002–4011, Sep. 2017.

[27] Y. Li, Z. Xu, J. Zhang, and K. P. Wong, "Variable gain control scheme of DFIG-based wind farm for over-frequency support," *Renew. Energy*, vol. 120, pp. 379–391, May 2018.

[28] M. Dreidy, H. Mokhlis, and S. Mekhilef, "Inertia response and frequency control techniques for renewable energy sources: A review," *Renew. Sustain. Energy Rev.*, vol. 69, pp. 144–155, Mar. 2017.

[29] S. I. Abouzeid, Y. Guo, and H.-C. Zhang, "Dynamic control strategy for the participation of variable speed wind turbine generators in primary frequency regulation," *J. Renew. Sustain. Energy*, vol. 11, no. 1, Jan. 2019, Art. no. 013304.

[30] M. Nadour, A. Essadki, and T. Nasser, "Coordinated control using back-stepping of DFIG-based wind turbine for frequency regulation in high wind energy penetrated system," *Math. Problems Eng.*, vol. 2020, pp. 1–16, Apr. 2020.

[31] C. Pradhan and C. N. Bhende, "Adaptive deloading of stand-alone wind farm for primary frequency control," *Energy Syst.*, vol. 6, no. 1, pp. 109–127, Mar. 2015.

[32] Y.-Q. Bao and Y. Li, "On deloading control strategies of wind generators for system frequency regulation," *Int. Trans. Electr. Energy Syst.*, vol. 25, no. 4, pp. 623–635, Apr. 2015.

[33] M. F. M. Arani and Y. A.-R.-I. Mohamed, "Dynamic droop control for wind turbines participating in primary frequency regulation in microgrids," *IEEE Trans. Smart Grid*, vol. 9, no. 6, pp. 5742–5751, Nov. 2018.

[34] Y. Liu, L. Jiang, J. S. Smith, and Q. H. Wu, "Primary frequency control of DFIG-WTs using bang-bang phase angle controller," *IET Gener., Transmiss. Distrib.*, vol. 12, no. 11, pp. 2670–2678, Jun. 2018.

[35] U. Datta, A. Kalam, and J. Shi, "Frequency performance analysis of multi-gain droop controlled DFIG in an isolated microgrid using real-time digital simulator," *Eng. Sci. Technol., Int. J.*, vol. 23, no. 5, pp. 1028–1041, Oct. 2020.

[36] K. V. Vidyanandan and N. Senroy, "Primary frequency regulation by deloaded wind turbines using variable droop," *IEEE Trans. Power Syst.*, vol. 28, no. 2, pp. 837–846, May 2013.

[37] L. Miao, J. Wen, H. Xie, C. Yue, and W.-J. Lee, "Coordinated control strategy of wind turbine generator and energy storage equipment for frequency support," *IEEE Trans. Ind. Appl.*, vol. 51, no. 4, pp. 2732–2742, Jul. 2015.

[38] F. Díaz-González, M. Hau, A. Sumper, and O. Gomis-Bellmunt, "Coordinated operation of wind turbines and flywheel storage for primary frequency control support," *Int. J. Electr. Power Energy Syst.*, vol. 68, pp. 313–326, Jun. 2015.

[39] K. E. Okedu, "A variable speed wind turbine flywheel based coordinated control system for enhancing grid frequency dynamics," *Int. J. Smart Grid-ijSmartGrid*, vol. 2, no. 2, pp. 123–134, Nov. 2018.

[40] I. Hamzaoui, F. Bouchafaa, and A. Talha, "Advanced control for wind energy conversion systems with flywheel storage dedicated to improving the quality of energy," *Int. J. Hydrogen Energy*, vol. 41, no. 45, pp. 20832–20846, Dec. 2016.

[41] A. Hutchinson and D. T. Gladwin, "Optimisation of a wind power site through utilisation of flywheel energy storage technology," *Energy Rep.*, vol. 6, pp. 259–265, May 2020.

[42] S. Wang, T. Wei, and Z. Qi, "Supercapacitor energy storage technology and its application in renewable energy power generation system," in *Proc. ISES World Congr.*, vols. 1–5. Berlin, Germany: Springer, 2008, pp. 2805–2809.

[43] J. Zhu, J. Hu, W. Hung, C. Wang, X. Zhang, S. Bu, Q. Li, H. Urdal, and C. D. Booth, "Synthetic inertia control strategy for doubly fed induction generator wind turbine generators using lithium-ion supercapacitors," *IEEE Trans. Energy Convers.*, vol. 33, no. 2, pp. 773–783, Jun. 2018.

[44] M. F. M. Arani and E. F. El-Saadany, "Implementing virtual inertia in DFIG-based wind power generation," *IEEE Trans. Power Syst.*, vol. 28, no. 2, pp. 1373–1384, May 2013.

[45] X. Zeng, T. Liu, S. Wang, Y. Dong, and Z. Chen, "Comprehensive coordinated control strategy of PMSG-based wind turbine for providing frequency regulation services," *IEEE Access*, vol. 7, pp. 63944–63953, 2019.

[46] B. Zakeri and S. Syri, "Electrical energy storage systems: A comparative life cycle cost analysis," *Renew. Sustain. Energy Rev.*, vol. 42, pp. 569–596, Feb. 2015.

[47] G. He, Q. Chen, C. Kang, Q. Xia, and K. Poolla, "Cooperation of wind power and battery storage to provide frequency regulation in power markets," *IEEE Trans. Power Syst.*, vol. 32, no. 5, pp. 3559–3568, Sep. 2017.

[48] R. Abhinav and N. M. Pindoriya, "Grid integration of wind turbine and battery energy storage system: Review and key challenges," in *Proc. IEEE 6th Int. Conf. Power Syst. (ICPS)*, Mar. 2016, pp. 1–6.

[49] U. Datta, A. Kalam, and J. Shi, "Battery energy storage system control for mitigating PV penetration impact on primary frequency control and state-of-charge recovery," *IEEE Trans. Sustain. Energy*, vol. 11, no. 2, pp. 746–757, Apr. 2020.

[50] M. Yoon, J. Suh, and S. Jung, "Development of BESS design plan for wind power system using short-term capacity factor," in *Advances in Greener Energy Technologies*. Singapore: Springer, 2020, pp. 749–759.

[51] A. M. Howlader, Y. Izumi, A. Uehara, N. Urasaki, T. Senjyu, and A. Y. Saber, "A robust H_∞ controller based frequency control approach using the wind-battery coordination strategy in a small power system," *Int. J. Elect. Power Energy Syst.*, vol. 58, pp. 190–198, Jun. 2014.

[52] S. M. Alhejaj and F. M. Gonzalez-Longatt, "Investigation on grid-scale BESS providing inertial response support," in *Proc. IEEE Int. Conf. Power Syst. Technol. (POWERCON)*, Sep. 2016, pp. 1–6.

[53] F. Díaz-González, A. Sumper, O. Gomis-Bellmunt, and R. Villafáfila-Robles, "A review of energy storage technologies for wind power applications," *Renew. Sustain. Energy Rev.*, vol. 16, no. 4, pp. 2154–2171, May 2012.

[54] G. Xu, J. Morrow, and L. Xu, "Power oscillation damping using wind turbines with energy storage systems," *IET Renew. Power Gener.*, vol. 7, no. 5, pp. 449–457, Sep. 2013.

[55] T. Mesbahi, A. Ouari, T. Ghennam, E. M. Berkouk, N. Rizoug, N. Mesbahi, and M. Meradji, "A stand-alone wind power supply with a Li-ion battery energy storage system," *Renew. Sustain. Energy Rev.*, vol. 40, pp. 204–213, Dec. 2014.

[56] L. A. G. Gomez, A. P. Grilo, M. B. C. Salles, and A. J. S. Filho, "Combined control of DFIG-based wind turbine and battery energy storage system for frequency response in microgrids," *Energies*, vol. 13, no. 4, p. 894, Feb. 2020.

[57] P. Cortes, M. P. Kazmierkowski, R. M. Kennel, D. E. Quevedo, and J. Rodriguez, "Predictive control in power electronics and drives," *IEEE Trans. Ind. Electron.*, vol. 55, no. 12, pp. 4312–4324, Dec. 2008.

[58] J. Rodriguez and P. Cortes, *Predictive Control of Power Converters and Electrical Drives*, vol. 40. Hoboken, NJ, USA: Wiley, 2012.

[59] W. Bao, Q. Wu, L. Ding, S. Huang, F. Teng, and V. Terzija, "Synthetic inertial control of wind farm with BESS based on model predictive control," *IET Renew. Power Gener.*, vol. 14, no. 13, pp. 2447–2455, Oct. 2020.

[60] M. Abdelrahem, C. M. Hackl, and R. Kennel, "Finite position set-phase locked loop for sensorless control of direct-driven permanent-magnet synchronous generators," *IEEE Trans. Power Electron.*, vol. 33, no. 4, pp. 3097–3105, Apr. 2018.

LUIS A. G. GOMEZ (Member, IEEE) received the degree in electronic engineering from the Industrial University of Santander (UIS), Bucaramanga, Colombia, in 2014, and the M.Sc. degree from the Federal University of ABC (UFABC), Santo André, Brazil, in 2016. He is currently pursuing the Ph.D. degree with the University of São Paulo (USP), São Paulo, Brazil, working in the areas of electrical power systems and wind energy.

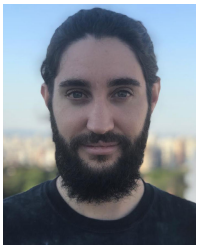

LUIS F. N. LOURENÇO (Member, IEEE) received the B.Sc. degree in electrical engineering with an emphasis in control systems and the M.Sc. degree in electrical engineering focused on power systems from the University of São Paulo (USP), São Paulo, Brazil, in 2014 and 2017, respectively, where he is currently pursuing the Ph.D. degree with the Polytechnic School of the University. His research interests include renewable energy, VSC-HVDC, modular multilevel converters, microgrids, future ancillary services, and nonlinear control.

AHDA P. GRILO (Senior Member, IEEE) received the bachelor's degree in electrical engineering from the State University of Western Paraná, in 2003, the master's and doctorate degrees in electrical engineering from the State University of Campinas, in 2005 and 2008, respectively, and the Ph.D. degree from the University of Alberta, in 2014. She is currently an Associate Professor with the Federal University of ABC (UFABC). She has experience in the area of electrical power systems, working mainly in the following topics: distributed generation, wind generation, connection of wind generators to the grid, stability of wind generators, and intelligent networks.

M. B. C. SALLES (Member, IEEE) received the M.Sc. degree from the State University of Campinas (UNICAMP), São Paulo, Brazil, in 2004, and the Ph.D. degree from the University of São Paulo (USP), in 2009. From 2006 to 2008, he joined the Research Team of the Institute of Electrical Machines, RWTH Aachen University. From 2014 to 2015, he was a Visiting Scholar at Harvard John A. Paulson School of Engineering and Applied Sciences. He is one of the founders of the Laboratory of Advanced Electric Grids (LGrid). He is currently an Assistant Professor with the Polytechnic School, USP. His main interests are in distributed generation, power system dynamics, control and stability, renewable energy, energy storage, and electricity markets.

LASANTHA MEEGAHAPOLA (Senior Member, IEEE) received the B.Sc. Eng. (Hons.) degree in electrical engineering (First Class) from the University of Moratuwa, Sri Lanka, in 2006, and the Ph.D. degree from the Queen's University of Belfast, U.K., in 2010. His doctoral study was based on the investigation of power system stability issues with high wind penetration, and research was conducted in collaboration with EirGrid (Republic of Ireland-TSO). He has over 14 years of research experience in power system dynamics and stability with renewable power generation and has published more than 100 journal and conference papers. He has also conducted research studies on microgrid dynamics and stability, and has coordinated reactive power dispatch during steady-state and dynamic/transient conditions for networks with high wind penetration. He was a Visiting Researcher with the Electricity Research Centre, University College Dublin, Ireland, in 2009 and 2010, respectively. From 2011 to 2014, he was employed as a Lecturer at the University of Wollongong (UOW), where he continues as an Honorary Fellow. He is currently employed as a Senior Lecturer at the Royal Melbourne Institute of Technology (RMIT) University. He is a member of the IEEE Power Engineering Society (PES). He is also an active member of the IEEE PES Power System Dynamic Performance (PSDP) Committee task force on microgrid stability analysis and modeling and the working group on voltage stability. He made key contributions toward identifying and classifying stability issues in microgrids. He is also serving as an Associate Editor for the IEEE Access and *IET Renewable Power Generation* journals.

A. J. SGUAREZI FILHO (Senior Member, IEEE) received the Ph.D. degree from Campinas University, Brazil, in 2010. He is currently a Professor with the Federal University of ABC (UFABC), Santo André, Brazil, teaching in the areas of electrical machines, power electronics, and electrical drives. His research interests are machine drives, wind and photovoltaic energies, and electrical power systems.